The 2nd National Conference on Electronics, Electrical Engineering, Telecommunications, and Computer Vision

C3ETCV'24, November 24-25, 2024,

Abdelhafid Boussouf University Centre of Mila, Algeria

Centre Universitaire de MILA

CERTIFICATE

Is awarded to

Bilal Djamal Eddine Cherif

For his/her excellence in presenting the research paper titled,

"Effects of DC Bus Short-Circuit Faults on the Electrical and Mechanical Performance of Induction Motors"

With co authors: Sara Seninete, Hilal Rahali

The director of institute

مدير معهد العلوم و التكنولوجيا

الأستاذ : كموخ سامي

Conference chair

Dr. Billel Smaani

Ministry of Higher Education an Scientific Research • University Centre of Abdelhafid Boussouf Mila •

The 2St National Conference on Electronics, Electrical Engineering Telecommunications And Computer Vision

Effects of DC Bus Short-Circuit Faults on the Electrical and Mechanical Performance of Induction Motors

Bilal Djamal Eddine Cherif[1], Sara Seninete[2] and Hilal Rahali[1]

[1]Electrical Engineering Laboratory (LGE), Department of Electrical Engineering, Faculty of Technology, University of M'sila, University Pole, Road Bourdj Bou Arreiridj, M'sila 28000 Algeria
[2]Department of Electrical Engineering, Faculty of Technology, University of Mostaganem, Mostaganem 27000, Algeria

cherif.bilaldjamaleddine@univ-msila.dz; saraseninete@gmail.com; hilal.rahali@univ-msila.dz

***Abstract*— This paper provides an in-depth analysis of the electrical and mechanical behavior of induction motors under DC bus short-circuit conditions. It introduces a novel detection method that utilizes the Hilbert-Huang spectral envelope of the stator current to identify and locate DC bus short-circuits. The simulation results confirm the effectiveness of this fault detection and localization approach, demonstrating its ability to address various operational degradations in induction motors caused by DC bus short-circuits.**

Keywords- Induction motor, inverter, fault, DC bus, FFT, ENV

I. INTRODUCTION

Electric drives comprising power supply, static converters, asynchronous machines, and loads are currently the most widely used tools for electromechanical conversion in industry. Their popularity stems from their simple construction, optimal maintenance and purchase costs, and mechanical robustness. Variable speed asynchronous machines are now applied in various fields, including aeronautics, robotics, and high-precision industrial mechanisms [1].

As these drives become more prevalent across diverse applications, issues related to aging and failure increasingly impact operational constraints. To enhance the reliability of systems that integrate inverter-asynchronous motor assemblies, the implementation of operational safety devices is often necessary. These measures help improve system availability, reduce maintenance costs, and ensure the safety of both equipment and personnel [2].

However, both electrical and mechanical equipment encounter a range of external and internal stresses throughout their lifespan, which can result in failure. The industrial sector places a strong emphasis on the reliability, maintainability, availability, and safety of these systems. As a result, there is an increasing focus on techniques for assessing the condition of these drives [3].

Significant advancements have been made in diagnosing variable-speed electric drives, particularly regarding asynchronous motor faults. These include issues such as the breakage of one or more consecutive rotor bars, damage to a portion of the short-circuit ring, short-circuits between turns in the windings, and various types of eccentricities. Additionally, faults in static converters (power supplies) have been addressed, including open circuit faults in IGBTs, short-circuit faults in *IGBTs*, phase insulation faults, and *DC* bus short-circuit faults [4].

Static converters (inverters) are essential components of variable speed electrical drive systems. Reliability data from the literature highlights the need to implement fault tolerance measures. The distribution of inverter faults is as follows: 60% are due to DC bus short circuits, 53% are due to control circuit issues, 38% arise from power circuit failures, 31% are linked to *IGBT* faults, 9% fall under other categories, and 6% are attributed to diode failures [5].

Several monitoring methods are based on a model of the system in question. The basic principle of these approaches is to compare the online data collected from the installation with a behavioral model. The effectiveness of the monitoring system largely depends on the quality of the model used. In some cases, the identification of faults may require the use of a model of the faulty system. Different levels of knowledge about the faults can be used, but it is important to note that obtaining an accurate model of the fault behaviour can often be difficult and expensive [6].

In recent years, a new technique known as Motor Current Signature Analysis (*MCSA*) has gained popularity. This method is particularly effective because the stator current holds valuable information about nearly all potential faults in inverter and induction motors. Analyzing stator currents in the frequency domain remains the most widely used approach, especially under steady-state conditions, as the resulting spectrum provides insights into the majority of electrical and mechanical faults that may arise within an inverter and induction machine assembly. [7].

within an inverter and induction machine assembly. The main advantage of this technique is its ability to detect a wide range of electromechanical faults using only the stator current and electromagnetic torque. This eliminates the need for

additional sensors dedicated to measuring mechanical quantities or vibrations. Another advantage is that current sensors are already integrated into all electric drive control systems, allowing for measurement without interrupting machine operation [10].

This paper focuses on the diagnosis and localization of faults associated with *DC* bus short-circuits in inverter and induction motor assemblies. It presents the use of the Hilbert-Huang spectral envelope of stator current to identify and pinpoint issues arising from these short-circuits. The simulation results demonstrate that this approach effectively detects and addresses various operational degradations in inverter and induction motor assemblies caused by *DC* bus faults.

II. INVERTER MODELING

Fig. 1, illustrates a block diagram of a two-level three-phase voltage inverter.

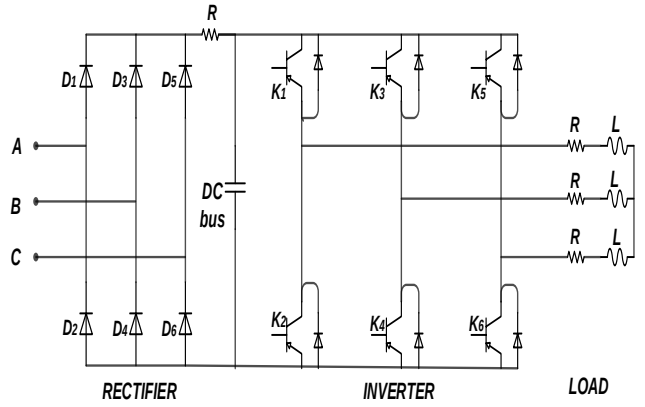

Figure. 1: Two-level three-phase voltage inverter.

The simplified diagram of the three-phase inverter shows a relationship between the phase-to-neutral voltages at points *A*, *B*, and *C* and their values relative to the midpoint (0). This relationship is expressed by the following matrix equation [11]:

$$\begin{bmatrix} V_A \\ V_B \\ V_C \end{bmatrix} = \frac{1}{3}\begin{bmatrix} 2 & -1 & -1 \\ -1 & 2 & -1 \\ -1 & -1 & 2 \end{bmatrix}\begin{bmatrix} V_{A0} \\ V_{B0} \\ V_{C0} \end{bmatrix} \quad (1)$$

The voltages V_A, V_B, and V_C represent the output voltages of the inverter used to supply and control the induction motor. Given that [12]:

$$\begin{cases} V_{A0} = \frac{E}{2} S_a \\ V_{B0} = \frac{E}{2} S_b \\ V_{C0} = \frac{E}{2} S_c \end{cases} \quad (2)$$

The control signals Si ($i = a, b$ and c) are given by:

$S_i = K_i$ is ***ON*** and K_i' is ***OFF***

$S_i = K_i$ is ***OFF*** and K_i' is ***ON***

The voltages output by the inverter are as follows:

$$\begin{bmatrix} V_A \\ V_B \\ V_C \end{bmatrix} = \frac{E}{3}\begin{bmatrix} 2 & -1 & -1 \\ -1 & 2 & -1 \\ -1 & -1 & 2 \end{bmatrix}\begin{bmatrix} S_a \\ S_b \\ S_c \end{bmatrix} \quad (3)$$

To determine the phase-to-phase voltages between two phases, use the following relationship [13]:

$$\begin{cases} V_{AB} = V_A - V_B \\ V_{BC} = V_B - V_C \\ V_{CA} = V_C - V_A \end{cases} \quad (4)$$

The relation between the vector $\left[S_a, S_b \text{ and } S_c\right]^T$ and the vector of line voltages $\left[V_{AB}, V_{BC} \text{ and } V_{CA}\right]^T$ is given by:

$$\begin{bmatrix} V_{AB} \\ V_{BC} \\ V_{CA} \end{bmatrix} = E\begin{bmatrix} 1 & -1 & 0 \\ 0 & 1 & -1 \\ -1 & 0 & 1 \end{bmatrix}\begin{bmatrix} S_a \\ S_b \\ S_c \end{bmatrix} \quad (5)$$

A. Inverter control

This article proposes a vector pulse width modulation (*PWM*) strategy, which involves the following steps [14]:

Step 01: Calculation of V_{ref} and q as functions of V_α and V_b using the following equation:

$$V_{ref} = \sqrt{V_\alpha^2 + V_\beta^2} \quad (6)$$

$$\theta = arctan\left(\frac{V_\beta}{V_\alpha}\right) \quad (7)$$

Step 02: Calculation of T_k , T_{k+1} and T_0 using the following equations:

$$T_0 = T_{MLI} - T_k - T_{k+1} \quad (8)$$

$$T_k = \sqrt{3}\frac{T_{MLI} V_{ref}}{E} sin\left(\theta + \frac{k}{3}\pi\right) \quad (9)$$

$$T_{k+1} = \sqrt{3}\frac{T_{MLI} V_{ref}}{E} sin\left(\theta - \frac{k-1}{3}\pi\right) \quad (10)$$

Step 03: Calculation of the on/off times for the six IGBTs by adjusting the duty cycle registers, as outlined in the following table:

TABLE I. ON/OFF TIMES

SECTORS	DUTY CYCLE
1	$t_{aon} = t_a + t_b + t_0 / 2$ $t_{bon} = t_b + t_0 / 2$ $t_{con} = t_0 / 2$
2	$t_{aon} = t_a + t_0 / 2$ $t_{bon} = t_a + t_b + t_0 / 2$ $t_{con} = t_0 / 2$
3	$t_{aon} = t_0 / 2$ $t_{bon} = t_a + t_b + t_0 / 2$ $t_{con} = t_b + t_0 / 2$
4	$t_{aon} = t_0 / 2$ $t_{bon} = t_b + t_0 / 2$ $t_{con} = t_a + t_b + t_0 / 2$
5	$t_{aon} = t_b + t_0 / 2$ $t_{bon} = t_0 / 2$ $t_{con} = t_a + t_b + t_0 / 2$
6	$t_{aon} = t_a + t_b + t_0 / 2$ $t_{bon} = t_0 / 2$ $t_{con} = t_a + t_0 / 2$

B. Induction motor model

The three-phase stator voltages of an induction machine, under balanced conditions, can be expressed as follows:

$$\begin{cases} V_a = \sqrt{2}V_{rms}\sin(\omega t) \\ V_b = \sqrt{2}V_{rms}\sin\left(\omega t - \frac{2\pi}{3}\right) \\ V_c = \sqrt{2}V_{rms}\sin\left(\omega t + \frac{2\pi}{3}\right) \end{cases} \tag{11}$$

The relationship between the αβ and a, b and c reference frames is given by the following equation:

$$\begin{bmatrix} V_\alpha \\ V_\beta \end{bmatrix} = \frac{2}{3}\begin{bmatrix} 1 & \frac{1}{2} & -\frac{1}{2} \\ 0 & \frac{\sqrt{3}}{2} & -\frac{\sqrt{3}}{2} \end{bmatrix}\begin{bmatrix} V_a \\ V_b \\ V_c \end{bmatrix} \tag{12}$$

The voltages on the direct and quadrature axes are then given by:

$$\begin{bmatrix} V_d \\ V_q \end{bmatrix} = \frac{2}{3}\begin{bmatrix} \cos\theta & \sin\theta \\ -\sin\theta & \cos\theta \end{bmatrix}\begin{bmatrix} V_\alpha \\ V_\beta \end{bmatrix} \tag{13}$$

The instantaneous values of the stator and rotor currents in a three-phase system are ultimately determined using the following transformation:

$$\begin{bmatrix} i_\alpha \\ i_\beta \end{bmatrix} = \begin{bmatrix} \cos\theta & -\sin\theta \\ \sin\theta & \cos\theta \end{bmatrix}\begin{bmatrix} i_d \\ i_q \end{bmatrix} \tag{14}$$

$$\begin{bmatrix} i_a \\ i_b \\ i_c \end{bmatrix} = \frac{2}{3}\begin{bmatrix} -\frac{1}{2} & -\frac{\sqrt{3}}{2} \\ -\frac{1}{2} & -\frac{\sqrt{3}}{2} \end{bmatrix}\begin{bmatrix} i_\alpha \\ i_\beta \end{bmatrix} \tag{15}$$

The equations for the various flux linkages are expressed as follows:

$$\begin{cases} \frac{d\psi_{qs}}{dt} = \omega_b\left[V_{qs} - \left(\frac{\omega_e}{\omega_b}\right)\psi_{ds} - \left(\frac{R_s}{X_{ls}}\right)\left(\psi_{mq} - \psi_{qs}\right)\right] \\ \frac{d\psi_{ds}}{dt} = \omega_b\left[V_{ds} - \left(\frac{\omega_e}{\omega_b}\right)\psi_{qs} - \left(\frac{R_s}{X_{ls}}\right)\left(\psi_{mq} - \psi_{ds}\right)\right] \\ \frac{d\psi_{qr}}{dt} = \omega_b\left[V_{qr} - \left(\frac{\omega_e - \omega_r}{\omega_b}\right)\psi_{dr} - \left(\frac{R_r}{X_{ls}}\right)\left(\psi_{mq} - \psi_{qr}\right)\right] \\ \frac{d\psi_{dr}}{dt} = \omega_b\left[V_{dr} - \left(\frac{\omega_e - \omega_r}{\omega_b}\right)\psi_{qr} - \left(\frac{R_r}{X_{ls}}\right)\left(\psi_{mq} - \psi_{dr}\right)\right] \end{cases} \tag{16}$$

Next, substitute the flux linkage values to calculate the currents:

$$i_{qs} = \frac{1}{X_{ls}}\left(\psi_{qs} - \psi_{mq}\right)X_{ml} = \frac{1}{\left[\frac{1}{X_m} + \frac{1}{X_{ls}} + \frac{1}{X_{lr}}\right]} \tag{17}$$

$$i_{qr} = \frac{1}{X_{lr}}\left(\psi_{qr} - \psi_{mq}\right) \tag{18}$$

$$i_{ds} = \frac{1}{X_{ls}}\left(\psi_{ds} - \psi_{md}\right) \tag{19}$$

$$i_{dr} = \frac{1}{X_{lr}}\left(\psi_{dr} - \psi_{md}\right) \tag{20}$$

Using the above equations, the electromagnetic torque and rotor speed can be determined as follows:

$$T_e = \left(\frac{3}{2}\right)\left(\frac{P}{2}\right)\left(\frac{1}{\omega_b}\right)\left(\psi_{ds}i_{qs} - \psi_{qs}i_{ds}\right) \tag{21}$$

$$\omega_b = \int\left(\frac{P}{2J}\right)\left(T_e - T_l\right) \tag{22}$$

Fig. 2, presents the simulation results for the inverter-induction motor system using the Space Vector Modulation (*SVM*) technique.

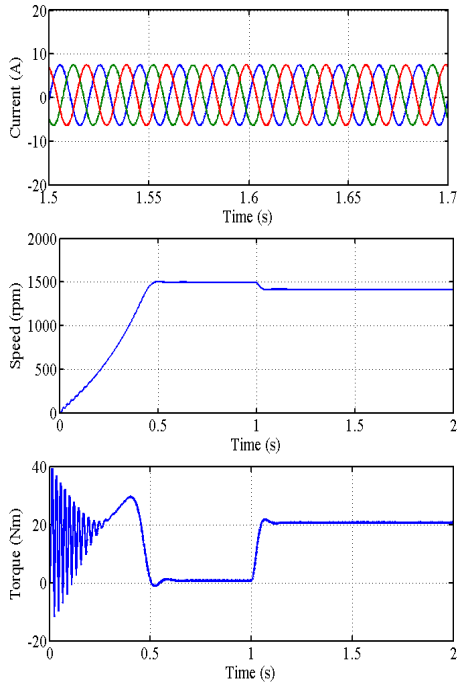

Figure. 2: Stator current, speed and torque in the case of healthy inverter.

We simulated an induction motor model connected to a voltage inverter controlled by the vector *PWM* technique under no load conditions. At t = 1s, a resistive torque of 20 Nm was applied. When comparing these results to those from a model without an inverter, we observe that while the overall trends are similar, there are noticeable oscillations around the average value. These oscillations are primarily attributed to harmonics present in the voltages supplied by the inverter.

C. Inverter with DC bus short-circuit

Faults upstream of the inverter, such as network-level issues or accidental grounding of one point on the *DC* bus, are generally outside the scope of this study. These faults are typically managed by contactors at the actuator input, which enable isolation of the system.

On the other hand, a *DC* bus short circuit can have various causes, such as connection faults or capacitor failures in the rectifier diodes. The effects of such a short circuit are similar to those experienced with a short circuit in the inverter leg. In the *AC* network, the actuator's contactors (for the induction motor) ensure isolation to prevent damage to the power generation system. Within the Rectifier-Inverter-Motor assembly, control functions cease as no voltage can be applied to the motor phases.

Blocking the inverter alone will not stop the current flow. In the simulations, we address this by opening the contactors and blocking the inverter immediately after a fault occurs. This action cancels all phase currents. Once the *DC* voltage drops below the threshold set by the electromotive force amplitude, the inverter switches to a three-phase diode bridge configuration. The amplitude of the phase currents then depends on the fault resistance; thus, if the fault resistance is low, the currents can be substantial. These currents produce a braking torque that decelerates the machine. The fault condition ends when the machine stops.

Fig. 3, presents the simulation results for a *DC* bus short circuit fault with a fault resistance of R_{sc}=0.1 Ω

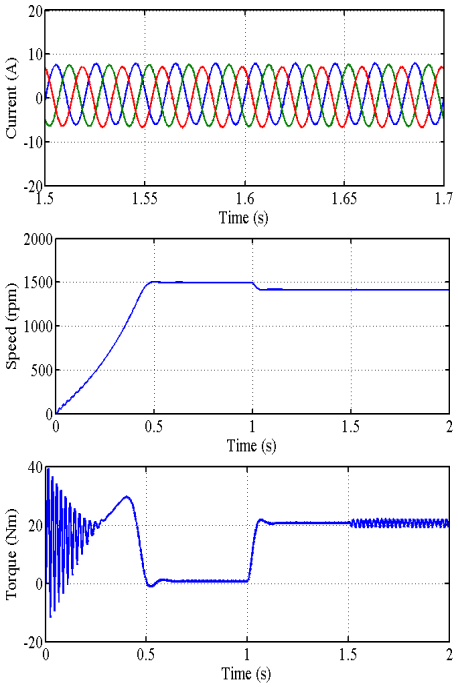

Figure. 3: Stator current, speed and torque in the case of faulty inverter with short-circuit R_{sc}=0.1 Ω.

Fig. 4, presents the simulation results for a *DC* bus short circuit fault with a fault resistance of R_{sc}=0.01 Ω

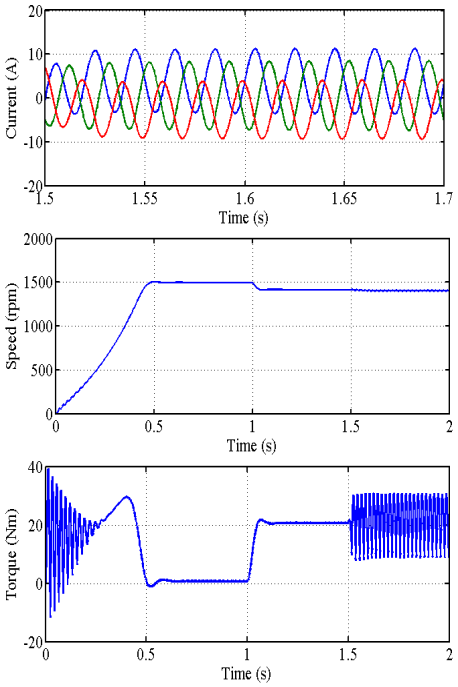

Figure. 4: Stator current, speed and torque in the case of faulty inverter with short-circuit R_{sc}=0.01 Ω.

The simulation results are illustrated in Figures 3 and 4 specifically show the curves for stator current, rotational speed, and electromagnetic torque.

In the abnormal regime, the onset of the degraded state leads to a transient imbalance in the currents, resulting in even higher intensity values. Additionally, this short-circuit condition is characterized by significant oscillations in both torque and stator current.

III. DETECTION TECHNIQUE BASED ON FFT AND ENV

In this section, we will explore two signal processing techniques.

A. Fast Fourier Transform algorithm (FFT)

Fig. 5 illustrates the fast Fourier transform algorithm.

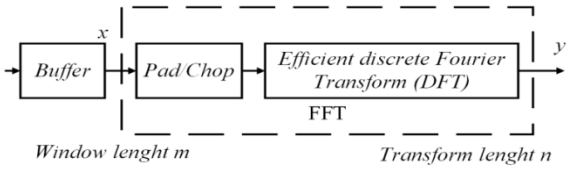

Figure. 5: Algorithm of FFT.

To implement the Fast Fourier Transform (FFT) for vectors of length N using MATLAB, follow the instructions provided in the equations below [15]:

$$y = fft(x) \tag{23}$$

Where:

$$x(k) = \sum_{j=1}^{N} x(j)\omega_N^{(j-1)(k-1)} \tag{24}$$

$$x(j) = \left(\frac{1}{N}\right) \sum_{j=1}^{N} x(k)\omega_N^{-(j-1)(k-1)} \tag{25}$$

$$\omega_N = e^{(-2\pi i)/N} \tag{26}$$

B. Envelope analysis (ENV)

The Hilbert transform of a signal $x(t)$ is defined by the following equation [16]:

$$H\left[x(t)\right] = \frac{1}{\pi} \int_{-\infty}^{+\infty} \frac{x(t)}{t-\tau} d\tau = \hat{x}(t) \tag{27}$$

Where: $\hat{x}(t)$ represents the imaginary component of the analytic signal and $z(t)$ which is defined as follows [16]:

$$z(t) = x(t) + j\,\hat{x}(t) = x(t) + jH\left[x(t)\right] = A(t)e^{j\varphi(t)} \tag{28}$$

Where: $H\left[x(t)\right]$ is the Hilbert transform of $x(t)$.

$$\varphi(t) = arctg\left[\frac{\hat{x}(t)}{x(t)}\right] \tag{29}$$

In practice, the envelope method involves several processing steps of the raw time signal before obtaining the final result. These steps are summarized below [17]:

Step 01: Filtering the raw signal to remove unwanted components;

Step 02: We use the Hilbert transform to compute the envelope;

Step 03: The envelope spectrum is calculated, from which fault information can be extracted.

Fig. 6, illustrates the FFT and ENV spectrum for both the healthy condition and the *DC* bus short circuit fault condition.

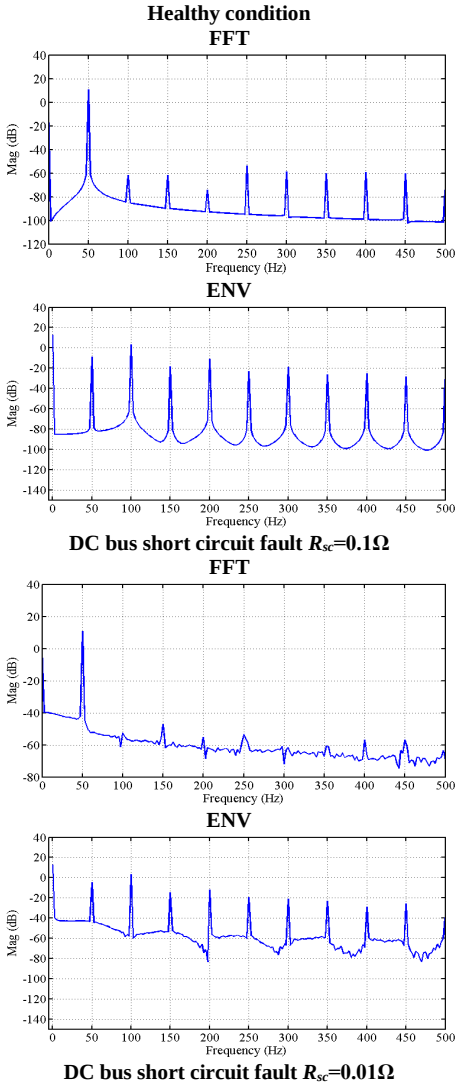

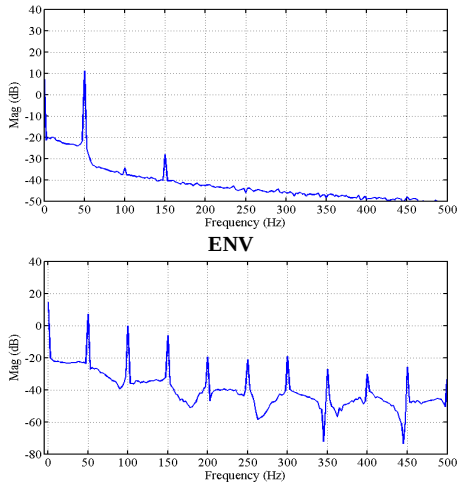

Figure. 6: FFT and ENV spectrum for both the healthy case and faulty case.

The key characteristics of Hilbert Huang's spectral envelope method are outlined as follows:

- Elimination of the fundamental frequency (50 Hz) from the current spectrum;
- Shift all frequency signatures left by 50 Hz;
- The removal of the fundamental frequency enhances the visibility of typically weak defect frequency signatures;
- The enhanced visibility of defect frequency signatures enables the use of a linear scale instead of a semi-logarithmic scale;
- By eliminating the fundamental frequency, a distinct frequency component characteristic of the fault is revealed, rather than the three multiple sidebands. This is exemplified by the signature of a *DC* bus short circuit fault.

The spectral analysis and spectral envelope of the stator current during a *DC* bus short-circuit fault are illustrated in Fig. 6. The FFT spectrum reveals the presence of f_s (50 Hz) and $3f_s$ (150 Hz). In the Hilbert-Huang spectral envelope, the fundamental harmonic f_s (50 Hz) is not visible due to the envelope effect, which enhances the visibility of other components and shifts all frequencies by 50 Hz. This shift explains the presence of the harmonic ($f_s + 2f_s$ = 150 Hz) at the frequency of $2f_s$ (100 Hz).

IV. Conclusion

This paper deals with the diagnosis and detection of *DC* bus short-circuits faults in a three-phase, two-level inverter-fed induction motor controlled by the *SVM* strategy.

Firstly, the effect of *DC* bus short-circuits faults on the inverter-induction motor system. Simulation results show that the current waveforms of the motor indicate it is not feasible to maintain long-term service continuity in the presence of a *DC* bus short-circuit fault.

The paper also introduces a diagnostic technique based on FFT and ENV for detecting *DC* bus short-circuit faults in inverters. The study specifically examines the harmonics present in the Hilbert-Huang spectral envelope, which may emerge in the spectrum as a result of these faults.

As perspectives, the following studies are focusing on distinguishing between DC bus short-circuit faults and inter-turn short-circuits in stator coils combining the signal processing techniques and artificial intelligence.

APPENDIX

Rated Power	3 KW
Supply frequency	50 Hz
Rated voltage	380 V
Rated current	7A
Rotor speed	1440 rev/min
Number of rotor bars	28
Number of stator slots	36
Power factor	0.83
Number of pair of poles	2

List of abbreviations

SVM: Space vector modulation;
PWM: Puse width modulation;
MCSA: Motor current signature analysis;
IGBT: Insulated gate bipolar transistors;
ENV: Envelope analysis;
FFT: Fast fourier transform.

List of symbols

$\boldsymbol{i}$: Sector number;
$\boldsymbol{E}$: DC voltage;
$\boldsymbol{V_{ref}}$: Reference vector;
$\boldsymbol{\theta}$: Angular position of the V_{ref};
$\boldsymbol{R_{sc}}$: Short-circuit resistance;
$\boldsymbol{N}$: Number of signal points;
$\boldsymbol{t}$: Variable time;
$\boldsymbol{f}$: Variable frequency;
$\boldsymbol{H[x(t)]}$: Hilbert transform of a signal *x(t)*;
$\boldsymbol{A(t)}$: Analytical signal module;
$\boldsymbol{\varphi(t)}$: Phase and instantaneous frequency of the signal;
$\boldsymbol{f_s}$: Fundamental frequency of the electrical network;
$\boldsymbol{P}$: Number of poles of Machine;
$\boldsymbol{T_e}$: Electromagnetic torque;

References

[1] I. Chouidira, D. Khodja, S. Chakroune " Continuous Wavelet Technique for Detection of Broken Bar Faults in Induction Machine" Traitement du Signal, Vol36, n:02,pp: 171-176.2019.

[2] S, Tianyu, C, Chaobo, W, Shenhang, et al. "Inverter open circuit fault diagnosis based on residual performance evaluation". IET Power Electronics, vol. 16, no 15, pp. 2560-2576, 2023.

[3] Z, Gang et YU, Jingrong. "Open-circuit fault diagnosis for cascaded H-bridge multilevel inverter based on LS-PWM technique". CPSS Transactions on Power Electronics and Applications, 2021, vol. 6, no 3, pp. 201-208, 2021.

[4] R, Saeed, T, Hadi, K, Naser Vosoughi, et al. "An overview of lifetime management of power electronic converters". Ieee Access, 2022, vol. 10, pp. 109688-109711, 2022.

[5] C, Bilal Djamal Eddine, B, Azeddine, et T, Mostefa. “An automatic diagnosis of an inverter IGBT open-circuit fault based on HHT-ANN”. Electric Power Components and Systems, 2020, vol. 48, no 6-7, pp. 589-602, 2020.

[6] F, JiSheng et Y, Wei. “Review of parametric fault prediction methods for power electronic circuits”. Engineering Research Express, vol. 3, no 4, pp. 042002, 2021.

[7] C, Chaobo, Y, Ying, Z, Binbin, et al. “The Diagnostic Method for Open-Circuit Faults in Inverters Based on Extended State Observer”. Mathematical Problems in Engineering, vol. 2021, no 1, pp. 5526173, 2021.

[8] L, Jin et Z, Youmin. “A diagnosis method of inverter open-circuit fault based on interval sliding mode observer ”. In : 2022 4th International Conference on Smart Power & Internet Energy Systems (SPIES). IEEE, pp. 604-608, 2022.

[9] H, Byong Jo, H, Dae Yeon, J, Pooreum, et al. “Offline Fault Diagnosis for 2-Level Inverter: Short-Circuit and Open-Circuit Detection”. Electronics, vol. 13, no 9, pp. 1672, 2024.

[10] C, Antonio J. Marques et B, Fernando. “Diagnostics and Fault Tolerance in DC–DC Converters and Related Industrial Electronics Technologies”. Electronics, vol. 12, no 10, pp. 2341, 2023.

[11] F, Masoud, V, Bhanu Teja, S, Rahman, et al. “ AC power cycling test setup and condition monitoring tools for SiC-based traction inverters”. IEEE Transactions on Vehicular Technology, vol. 72, no 10, pp. 12728-12743, 2023.

[12] A, Naser Pour, V, Bastian, et Z, Thomas. “An Innovative Method for Short Circuit Protection of a Three-Phase MOSFET Power Inverter”. In : 2023 IEEE Transportation Electrification Conference & Expo (ITEC). IEEE, pp. 1-4, 2023.

[13] T, Osman et Y, Deniz. “Analog dv/dt and di/dt Controlled Gate Driver With Self-Triggered Hold-at-Zero Algorithm for High-Power IGBTs”. IEEE Transactions on Power Electronics, vol. 39, no 1, pp. 1184-1194, 2023.

[14] L, Tian, H, Zhang, B, Hu, et al. “Fault diagnosis of three-level inverter based on convolutional neural network and support vector machine”. Journal of the Chinese Institute of Engineers, vol. 46, no 8, pp. 829-838, 2023.

[15] C, Bilal Djamal Eddine, B, Azeddine, et S, Sara. Induction Motor Diagnosis with Broken Rotor Bar Faults Using DWT Technique. In : 2021 International Conference on Electrical, Communication, and Computer Engineering (ICECCE). IEEE. pp. 1-5, 2021.

[16] C, Bilal Djamal Eddine, S, Sara, et D, Mabrouk. “A novel, machine learning-based feature extraction method for detecting and localizing bearing component defects”. Metrology and Measurement Systems, vol.29, no 2, pp. 333-346, 2022.

[17] C, Bilal Djamal Eddine, C, Mohamed, S, Sara, et al. “Machine-learning-based diagnosis of an inverter-fed induction motor”. IEEE Latin America Transactions, vol. 20, no 6, p. 901-911, 2022.